# Carbon Nanotube Bags: Catalytic Formation, Physical Properties, Two-Dimensional Alignment and Geometric Structuring of Densely Filled Carbon Tubes

**Jörg J. Schneider,*[a] Jörg Engstler,[a] Steffen Franzka,[a] Kathrin Hofmann,[b] Barbara Albert,[b] Jürgen Ensling,[c] Philipp Gütlich,[c] Peter Hildebrandt,[d] Susanne Döpner,[d] Wilhelm Pfleging,[e] Bernd Günther,[f] and Günter Müller[f]**

**Abstract:** The catalytic CVD synthesis, using propyne as carbon precursor and $Fe(NO_3)_3$ as catalyst precursor inside porous alumina, gives carbon nanotube (CNT) bags in a well-arranged two-dimensional order. The tubes have the morphology of bags or fibers, since they are completely filled with smaller helicoidal CNTs. This morphology has so far not been reported for CNTs. Owing to the dense filling of the outer mother CNTs with small helicoidal CNTs, the resulting CNT fibers appear to be stiff and show no sign of inflation, as sometimes observed with hollow CNTs. The fiber morphology was observed by raster electron microscopy (REM), transmission electron microscopy (TEM), and atomic force microscopy (AFM). The carbon material is graphitic as deduced from spectroscopic studies (X-ray diffraction, Raman and electron energy-loss spectroscopy (EELS)). From Mössbauer studies, the presence of two different oxidation states ($Fe^0$ and $Fe^{III}$) of the catalyst is proven. Geometric structuring of the template by two different methods has been studied. Inkjet catalyst printing shows that the tubes can be arranged in defined areas by a simple and easily applied technique. Laser-structuring creates grooves of nanotube fibers embedded in the alumina host. This allows the formation of defined architectures in the μm range. Results on hydrogen absorption and field emission properties of the CNT fibers are reported.

**Keywords:** carbon · catalyst · CVD · iron · nanostructures

[a] Prof. Dr. J. J. Schneider,[+] Dipl. Chem. J. Engstler,[+] Dr. S. Franzka
Institut für Anorganische Chemie der Universität/GH-Essen
Universitäts-strasse 5–7, 45117 Essen (Germany)

[+] Current address:
Institut für Chemie, Anorganische Chemie
Karl-Franzens-Universität Graz, Schubertstrasse 1
8010 Graz (Austria)
Fax: (+43) 316-380-9835
E-mail: joerg.schneider@uni-graz.ac.at

[b] Dipl. Chem. K. Hofmann, Dr. B. Albert
Institut für Anorganische und Analytische Chemie
Justus-Liebig-Universität Giessen (Germany)

[c] Dr. J. Ensling, Prof. Dr. P. Gütlich
Institut für Anorganische und Analytische Chemie
Johannnes-Gutenberg-Universität Mainz (Germany)

[d] Prof. Dr. P. Hildebrandt, Dr. S. Döpner
Max-Planck-Institut für Strahlenchemie
Stiftstrasse 3-6, 45470 Mülheim an der Ruhr (Germany)

[e] Dr. W. Pfleging
Forschungszentrum GmbH Technik und Umwelt, Karlsruhe
Institut für Materialforschung I, 76021 Karlsruhe (Germany)

[f] Dipl. Phys. B. Günther, Prof. Dr. G. Müller
Fb Physik, Bergische Universität/GH Wuppertal
42097 Wuppertal (Germany)

## Introduction

The properties of carbon nanotubes (CNTs) or carbon nanofibers vary with the experimental conditions in their formation processes.[1] Both carbon materials are composed of a number of carbon shells. However, a characteristic difference between a carbon nanotube and a vapor grown carbon fiber is that the former is hollow inside, whereas the latter is compact and dense. Nevertheless, dense and compact filling of originally hollow CNTs have already been achieved by introducing a guest, for example, semimetals, metals, and metal oxides.[1] Since the early 1950s, filamentary carbon fibers have emerged into a useful class of materials with unique mechanical properties. Although only known for one decade, CNTs promise versatile and unique properties in areas such as lithium-ion batteries,[2] fuel cells,[3] hydrogen storage,[4–8] or field emission applications.[9–11] For the last application, some challenges such as precise spatial alignment, uniform emission properties, and low-processing temperature must be met.

The template approach to CNTs, which involves the use of openings and pores of inorganic templates, allows the size and

  0947-6539/01/0713-2888 $ 17.50+.50/0 

shape of CNTs and fibers to be controlled. These techniques entail the use of lamellae of clays, for example, montmorillonite[12] or taeniolite,[13] or a template membrane with pores of uniform diameter.[14–18] Recently we reported the use of nanosized Fe/Fe oxide core/shell particles prepared by a solution-based organometallic route for the preparation of aligned carbon nanotubes.[19]

Herein we report on a new type of carbon nanotubes, which we refer to as CNT bags or fibers due to their unusual dense and compact filling with smaller, multi-walled helicoidal CNTs. Their formation is achieved by using an inorganic-template approach, employing catalytic amounts of an iron-based catalyst and propene as carbon precursor in a single-step CVD process.

## Results and Discussion

Impregnating Anopore® membrane discs (200 nm diameter) with an ethanolic $Fe^{III}(NO_3)_3$ solution (0.1 mol), followed by drying and reducing for 5 h at 500 °C under $H_2/N_2$, produces metallic iron (20%) ($\delta = 0.108$ mm s$^{-1}$, $H = 346$ kG, 4.2 K) within the pores of the template membrane [Eq. (1)]. However, (80% of) the remaining iron particles are still in the oxidation state +3 ($\delta = 0.51$ mm sec$^{-1}$, $H = 526 - 472$ kG, 4.2 K) as revealed by Mössbauer spectroscopy, indicating a partly reduced metal catalyst precursor (Figure 1). The two magnetic sextets characterizing the oxidic phases display a broad background, reflecting a wider particle size distribution. Thus we conclude that the hydrogen reduction procedure gives a catalyst that contains two active oxidation states of iron ($Fe^0$ and $Fe^{III}$). It is well known that if a metal catalyst precursor is evenly dispersed in an inorganic host material, it is considerably more difficult to be completely reduced.[20]

$$2\,[Fe(NO_3)_3@Anopore] \xrightarrow{500\,^\circ C} Fe_2O_3 + 6\,NO + 1.5\,O_2$$
$$\xrightarrow{3\,H_2,\ 500\,^\circ C} 2\,Fe^0_{minor} + 3\,H_2O \qquad (1)$$

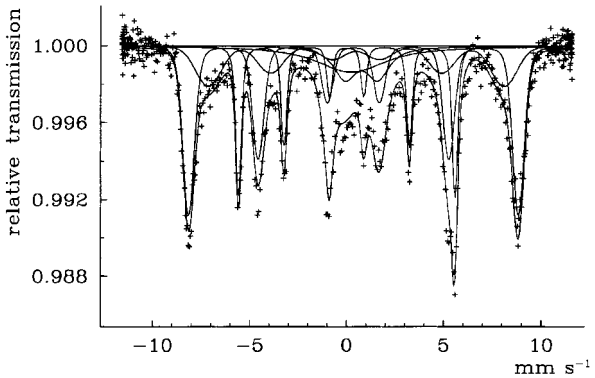


Figure 1. $^{57}$Fe Mössbauer spectrum (4.2 K) of a $Fe(NO_3)_3$ precatalyst impregnated, oxidized, and subsequently $H_2/N_2$ reduced Anopore® membrane.

For our CVD experiments, the Anodisc® membrane, containing the aforementioned reduced catalyst, was treated with a propene/$N_2$ mixture for 5 min. After pyrolysis, a brown/black membrane formed, and scanning electron microscopy (SEM) revealed a parallel arrangement of CNTs (Figure 2).

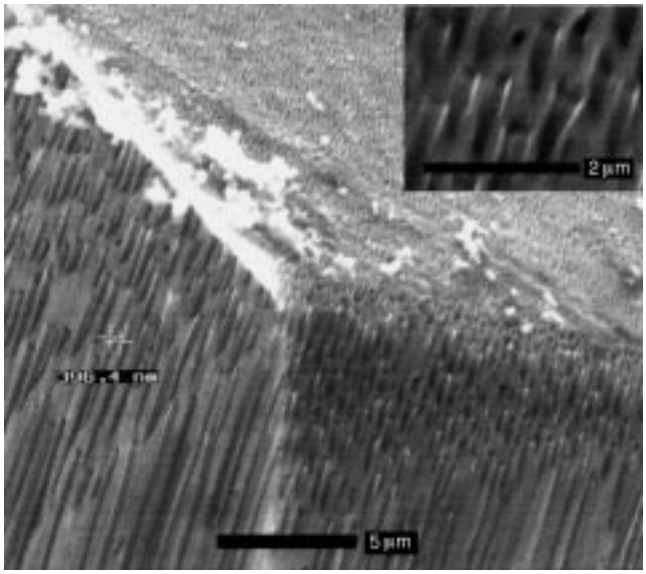


Figure 2. SEM of a typical block arrangement of CNTs obtained from the CVD experiment. Insert: edge view of the same sample showing the CNTs protruding out of the alumina membrane.

Drastically higher gas flow rates produced polycyclic aromatic hydrocarbons such as naphthalene and phenanthrene as additional off-stream gas pyrolysis products. These were isolated and subsequently characterized by NMR spectroscopy. Aside from the uniform, highly aligned, parallel arrangement of large areas of CNTs, additional characteristic features are present: nearly all pores are filled with CNTs and these have the same outer diameter as those of the pores of the template membrane. These features are characteristic for carbon nanotubes formed by the alumina template method employed herein.[17] Dissolving the alumina template in concentrated HF leaves the carbon tubes intact, but dissolves the alumina membrane. The parallel arrangement of the unchanged carbon nanotubes obtained displays a negative replica of the dissolved membrane. This is shown by SEM of the alumina-free CNTs (Figure 3).

The dramatic effect of the metal catalyst on the formation temperature of the CNTs can be seen when the $Fe(NO_3)_3$ catalyst precursor is loaded in confined areas of the alumina membrane by an inkjet printing technique. This enables the comparison between the temperature dependence of the CNT formation of a blank catalyst-free alumina area and a catalyst-impregnated area of the same alumina membrane in a single carbonization experiment. Figure 4a reveals that already at 650 °C, the catalyst impregnated Anopore® membrane produces spatially arranged CNTs in such areas where the catalyst was filled in the pores by the inkjet printing technique. In contrast to catalyst-impregnated areas, catalyst-free regions of the alumina membrane start to form CNTs inside the pores at temperatures no lower than 800 °C, (see Figure 4b).

  0947-6539/01/0713-2889 $ 17.50+.50/0 

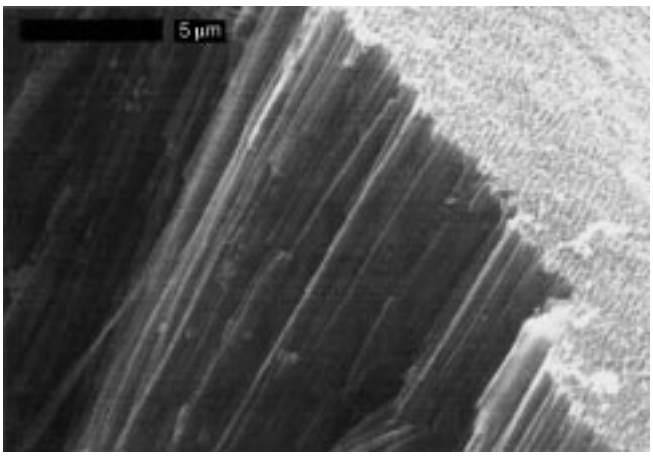


Figure 3. Free-standing parallel arrangment of CNTs after the alumina template has been dissolved with 48 % HF.

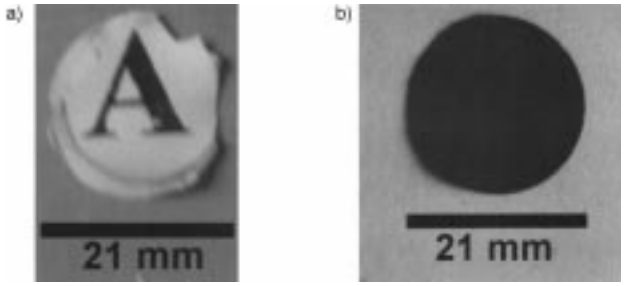


Figure 4. a) Alumina-embedded CNTs obtained by catalyst impregnation of the membrane by an inkjet printing technique followed by CVD of propene at 650 °C; b) the same membrane after raising the deposition temperature to 800 °C.

We studied the possibility of laser-assisted patterning of the alumina-embedded CNT fibers. The material processing was performed with excimer laser radiation (wavelength $\lambda =$ 248 nm, pulse length $\tau = 20$ ns) with an Exitech PS2000 micro-machining system. Figure 5 shows a series of patterns displaying ten linear grooves, with a width of around 10 µm and a length of 200 µm. The distance between the grooves is 30 µm in each block arrangement. For the ablation experiments, we used a demagnification of 25:1 and the laser fluences were varied between 0.5 J cm$^{-2}$ and 4 J cm$^{-2}$. There were 100 laser pulses (248 nm, procession gas: air) at a repetition rate of approximately 10 Hz. For the demagnification, a mask structure containing the groove arrangement displayed in Figure 5 was used.

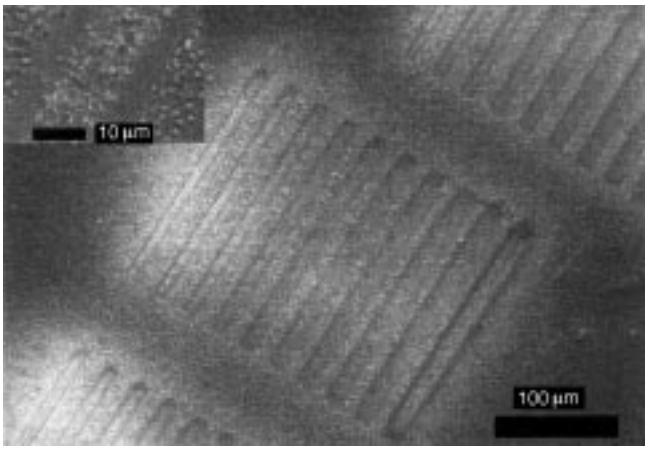


Figure 5. SEM of a ten block pattern of parallel grooves obtained from Anopore® embedded CNTs by laser structuring. Insert: two laser-created grooves; middle: unaltered CNT filled Anopore® region.

SEM of three parallel channels inside a single block shows a disordered arrangement of CNTs that grow out of the membrane surface and curl outside in an unstructured way (Figure 5). This curling of the CNTs on the surface of the membrane is due to the CVD growth process, which continues on the outer membrane surface in a disordered manner as a result of the lack of the template-ordering effect operating inside the Anopore® membrane. Both the left and right side of the pattern show the channels produced by the laser ablation process. The laser beam directly evaporates the alumina/carbon composite material. The observed debris formation is caused by redeposition of ablated material. This effect may be reduced under special ambient conditions (e.g., using He as processing gas or ablation in vacuum). However, unaltered areas containing the prepared, intact carbon material are obtained. Due to the high speed and precision to which laser-patterning process has already been developed,[21] large, structured areas should be accessible with alumina CNT fiber material.

Sonication of the parallel-arrangment of two-dimensional carbon nanotubes, obtained from the HF-treated template, in ethanol for several minutes produces a stable homogeneous dispersion. Transmission electron microscopy (TEM) of these dispersions still reveals bundles that display the parallel-arrangement of CNTs, but in addition single, disordered CNTs also become visible (Figure 6). TEM reveals that these tubes are completely filled with smaller diameter, multi-walled tubes. These smaller helicoidal multi-walled CNTs

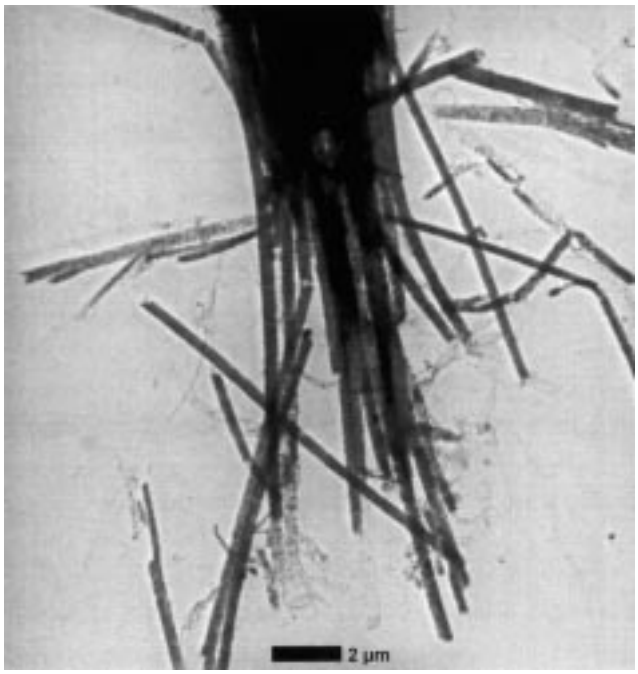


Figure 6. TEM of CNT fibers. The fiberlike, compact nature of the filled tubes is visible from the dark contrast of the single objects.



0947-6539/01/0713-2890 $ 17.50+.50/0 *Chem. Eur. J.* **2001**, *7*, No. 13

have a diameter of between 20 and 40 nm as measured by TEM (Figures 7 and 8). The possibility of a dense and nearly complete filling of vapor grown CNTs with smaller diameter coiled carbon tubes to yield a unique fiber-type morphology has not been reported. So far, only the incorporation of single CNTs in larger outer CNTs has been observed among the products of metal-catalyzed CVD deposition experiments of gaseous carbon precursors.[22, 23] Due to the irregular pore diameter of the commercial Anopore® membranes, the resulting CNT fiber nanotube radii vary over a wider range.

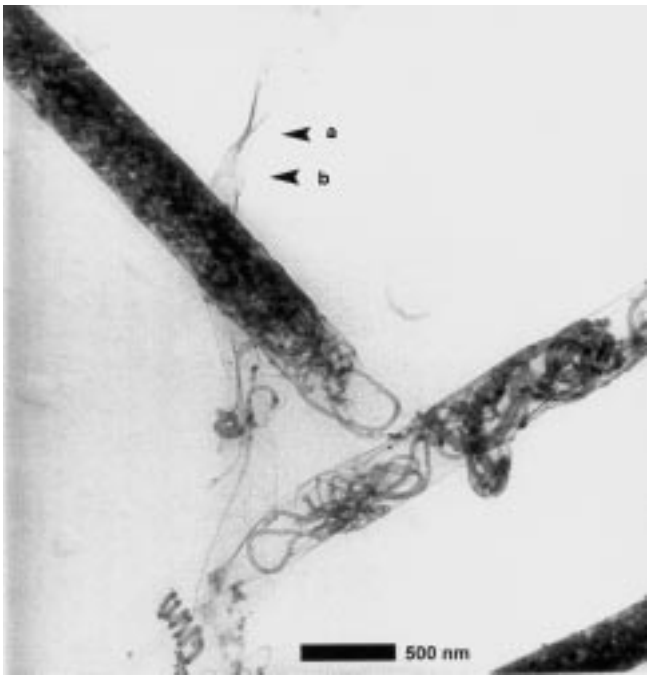


Figure 7. TEM of CNT fibers showing the dense, compact filling of the outer larger CNTs with smaller helicoidal CNTs. The arrows mark a flat and twisted region of an empty, collapsed CNT.

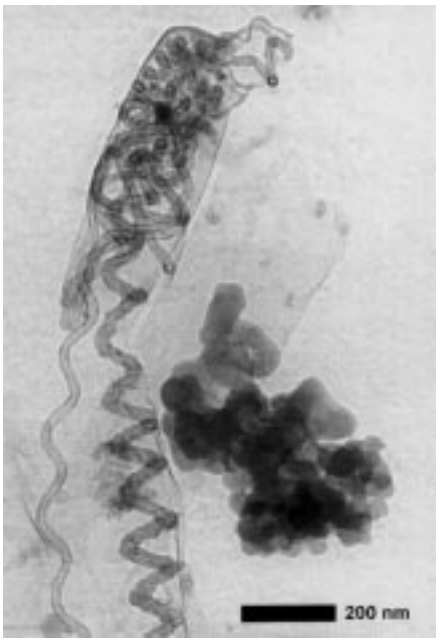


Figure 8. TEM of a outer CNT end with inner helicoidal CNT filling.

Two processes seem to be responsible for the formation of the CNT fiber morphology. Firstly, the outer larger diameter tubes are templated by the pores in the membrane. Secondly, the inside decoration with smaller CNTs is due to the Anopore®-encapsulated metal-catalyst particles, which serve as nucleation sites for the helical tube growth. Evidently under the chosen reaction conditions, the reactive carbon species formed from the precursor gas are available in sufficient quantities to enable tube growth: a) in a straight fashion on the alumina pore walls, and b) by diffusion of the reactive carbon species through the catalytic particles present inside the alumina pores as proposed by Baker.[24] Diffusion parameters of the reactive carbon species depend critically on particle size, type of hydrocarbon, gas-flow rate, and temperature.[1b] As a result of this dependence, different filament forms with different morphologies, for example, helicoidal, are to be expected from a carbon diffusion process. Helicoidal CNTs have been observed among the products obtained by pyrolysis of ethyne over a cobalt catalyst.[25] Since the accretion of carbon atoms occurs on the metal surface of the catalyst particles, their size and shape is important. As a result, different rates of carbon-species agglomeration arise within the CNT walls, thus giving rise to a helicoidal CNT structure.

Usually hollow carbon nanotubes are very flexible, for example, they have a high Young's modulus.[20] However, hollow CNTs can suffer a complete tube collapse along their length.[26] So far, we have not observed such collapsing phenomena with the dense, filled CNT fibers. CNT fibers appear to be stiff and rigid owing to their dense interior filling. However, aside from the CNT fiber morphology, we have also frequently observed long ribbonlike structures.[26] The structure of these ribbonlike tubes is dramatically different from our filled CNT fibers. The arrows in Figure 7 identify a particular flat "tube" structure. The region of the structure apparently lying flat against the TEM grid is marked "b" in Figure 7, whereas "a" denotes the twisted (perpendicular) region of the flat, collapsed structure.

The CNT fibers were also imaged in air with an atomic force microscope operating in the tapping mode (TM-AFM). Figure 9a–c shows different CNT fibers morphologies, and Figure 9d–f displays TM-AFM images of tube morphologies observed only occasionally. Figure 9a displays a bundle of two CNT fibers in an ideal parallel arrangement. Figure 9b shows the end part of a CNT fiber with a large amount of branching at the fiber end. This branching characterizes the alumina-membrane template morphology at the very end of the template membrane.[27] Figure 9c show a compact, densely filled, single CNT fiber. The measured height of this fiber is in the range 280–290 nm. Figure 9d displays a flat, fully collapsed CNT. The completely collapsed and flat inner part forces the remaining tube shell to form into two parallel smaller tubelike arrangements. From the height measurements at the end of the entire tube, the tube wall thickness was determined to be approximately 5 nm. From the circumference of the collapsed tube, the diameter of the original, noncollapsed tube was estimated to be 380 nm. Figure 9e, f displays the twisting and crumbling that occurs when a flat ribbonlike tube is lies over a compact and densely filled CNT

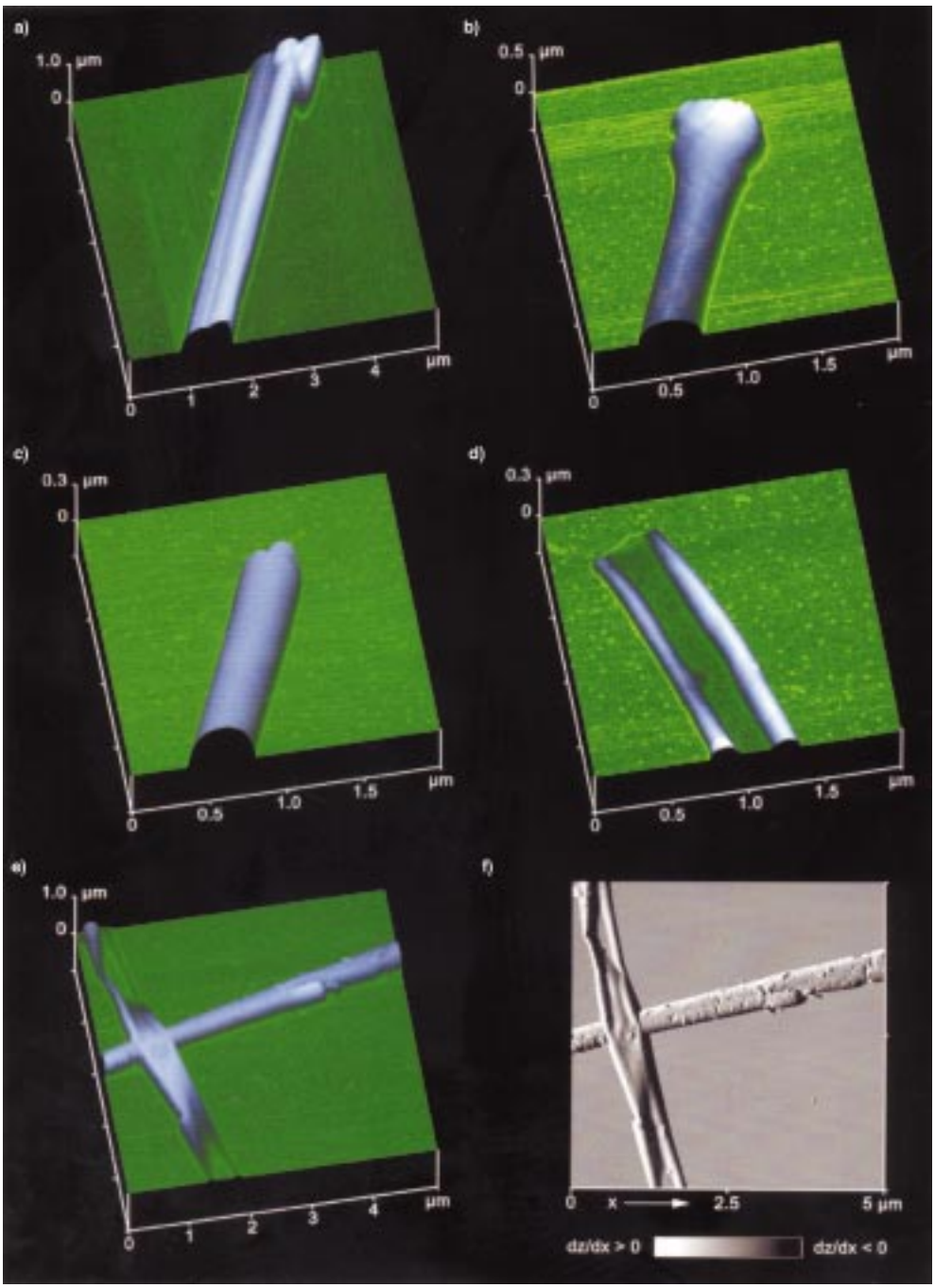


Figure 9. TM-AFM images of CNT fibers. Images a)–e) are pseudo-three-dimensional presentations of different topographies. A combination of color-coded height and illumination encoding was used to display the topographical information. e) is displayed as if a light source is shining on the topography from the right side. f) shows a surface plot of the height gradient dz/dx of the topography image.

fiber. Evidently the collapsed "tube" is prone to a high degree of twisting and bending, as is a flat ribbon, reflecting the high elasticity that such a collapsed tube has. For example, whilst lying across the CNT fiber, the collapsed tube undergoes a height difference of approximately 330 nm measured from the substrate to the top of the filled fiber without further mechanical damage.

In general, it should be noted that the lateral dimensions obtained from the AFM measurements may be affected by an imaging artifact known as tip convolution. Especially for large structures, such as CNT fibers, the measured lateral dimensions appear to be larger than the real ones because of the convolution between sample and tip geometry.[25] This effect is illustrated in Figure 10. Note that the measurement of the height would be not affected by this. Therefore, the diameter of a CNT fiber should be determined from the height and/or with respect to the really well-known tip geometry.

The graphitic nature of the CNT fibers (as prepared at 800 °C) was deduced from Raman spectroscopy, X-ray diffraction (XRD), and electron energy-loss spectroscopy (EELS). Raman spectroscopy[29] reveals two prominent graphitic peaks ($D = 1344\ cm^{-1}$, $G = 1529\ cm^{-1}$) in an inten-



0947-6539/01/0713-2892 $ 17.50+.50/0 *Chem. Eur. J.* **2001**, *7*, No. 13

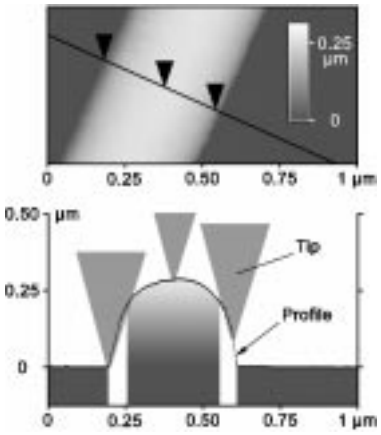


Figure 10. AFM imaging artifact while scanning a CNT fiber. Due to tip convolution, some parts of the measured topography would be dominated by the shape of the AFM tip. The displayed line profile results from a cross section through the image of a filled CNT fiber seen in the gray scale image. The part of the profile affected by the tip shape is indicated by the white areas under the line profile. Note that the tip shape may not affect the measurements on top of the fiber.

sity ratio of $I_D/I_G = 0.6$. This corresponds well to the ratio of low-crystallinity aligned CNTs, which were obtained on a porous silicate substrate by CVD techniques ($I_D/I_G = 0.8$).[30] The high intensity of the D peak, responsible for the high $I_D/I_G$ ratio, might be due to defects in the curved graphene sheets and tube ends in agreement with the nonuniform character of the CNTs as revealed by TEM. Powder diffraction of the CNT fiber material showed the characteristic graphitic 002 and 110 Bragg reflections as broad and intense peaks typical for a graphitlike structure.

EELS allows the determination of the relative amount of $sp^2$ and $sp^3$ bonding in carbon materials.[31] In such a measurement, excitations of the core electrons into unoccupied states with $C_{2p}$ character are probed. A comparison of the EELS of our CNT fiber arrangements with highly oriented pyrolitic graphite (HOPG) reveals subtle but significant changes in the spectral energies of the sharply defined π* and σ* features. The overall spectral feature of the complete EELS energy region is the same for HOPG and our CNT fibers arrangements. The low-loss region is significantly shifted towards lower energy compared to HOPG, indicating that a loss of valence electrons is most likely related to the tubular nature of the graphitic layers (Figure 11).[32] The core loss energy region displays signals corresponding to π* and σ* states, both of which are shifted to lower energies relative to HOPG.

Hydrogen absorption on carbon materials has been known for many years.[1a] During the last years, tremendous storage capacities of hydrogen have been reported for various CNT materials.[4–7] We investigated the storage capacity of our CNT fiber arrangements gravimetrically under isothermal conditions at 24 °C. The hydrogen absorption rate was calculated by the mass increase ($\Delta m$ in wt %) divided by the sample weight and was found to be 0.13 wt % (±0.08 %). This is in accord with a number of other carbon fiber and CNT materials measured by using the same technique.[32] Assuming a mainly physical absorption, this value corresponds to an active surface of around 500 $m^2 g^{-1}$. However, BET measurements

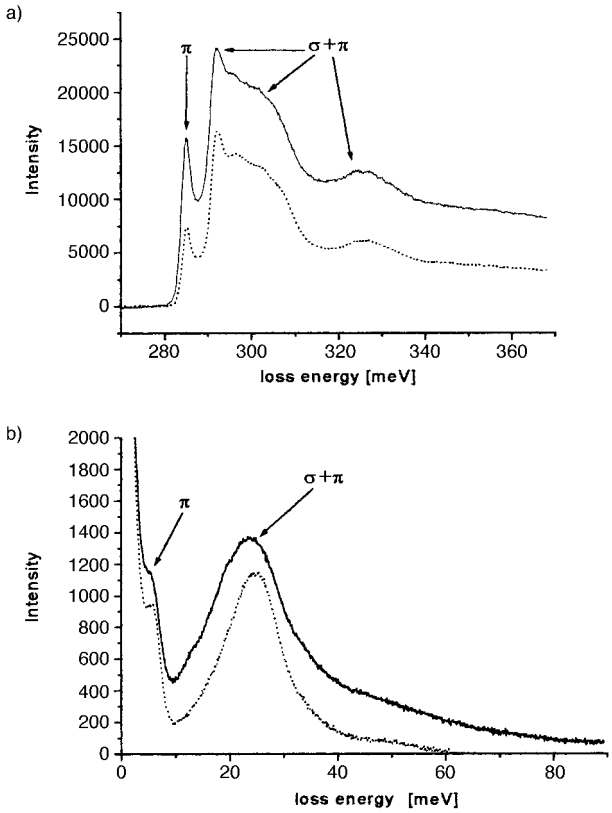


Figure 11. EEL spectra: a) $C_{1s}$ low-loss region; and b) core-loss region of CNT fibers compared to HOPG. Upper trace: CNT fibers; lower trace: HOPG.

of the CNT fiber material after $H_2$ loading experiments revealed a BET surface of only 50 $m^2 g^{-1}$. This is a significantly lowered surface area, possibly due to a break down of the tube wall structure.

CNTs can show field emission (FE) at electric fields below 10 V µm$^{-1}$, as a result of their high geometric field enhancement.[9–11] They are therefore promising candidates for applications as cold cathodes, for example, in flat panel displays and high intensity light sources.[10] Free-standing CNTs, however, are often lacking parallel alignment and provide limited thermal and mechanical stability.[11] The FE properties of our aligned CNT fibers were investigated by means of a field emission scanning microscope with a spatial resolution of several milimetres. At a few spots in the samples, a rather unstable FE current of about 10 nA was obtained at macroscopic fields between 5–125 V µm$^{-1}$. In situ SEM analysis revealed irregular surface structures occurring at some edges of the template present at the FE spots. The maximum geometric field enhancement of single CNT fibers can be estimated by their aspect ratio, that is, the height of the template divided by the pore diameter. This results in a value of about 400, which would cause FE at macroscopic fields around 10 V µm$^{-1}$. Since nearly all of the holes of the template are filled, the mutual electric shielding of the CNTs leads to a drastic reduction of the geometrical field enhancement, thus increasing the onset field of FE for the regular structure. In turn, edges with partially freed CNT fibers can be assumed to cause the observed FE.

## Conclusion

In summary we have shown that a new morphology of CNTs, CNT bags or fibers, can be prepared in a single step by using a CVD technique that employs a catalytic process. Their parallel alignment is possible by a standard template technique. Due to the dense filling of the outer mother CNTs with small helicoidal CNTs in their interior, the resulting CNT fibers appear to be stiff and show no sign of inflation, as observed with hollow CNTs. We are currently studying the physical (FE application) and mechanical properties of these and other CVD produced carbon materials in more depth.

## Experimental Section

**Catalyst precursor loading**: $Fe(NO_3)_3$ in ethanol (3 mL, 0.1M) was added dropwise on the surface of a Anodisc® membrane. Sufficient time was allowed for complete solvent evaporation after each catalyst precursor addition.

**CNT fibers formation process**: After complete solvent evaporation, the resulting intrinsic red/brown membrane was placed in a quartz tube (30 cm, 3.0 cm diameter, in a furnace of a CVD experimental setup)[19] perpendicular to the gas flow. An $N_2$ purge (22.5 $L\,h^{-1}$) was maintained for 20 min. After reducing the $N_2$ flow to 2.0 $L\,h^{-1}$, the furnace was heated to 550 °C and an $H_2$ flow of 4.0 $L\,h^{-1}$ was maintained in addition to the $N_2$ flow for 2 h. The $N_2$ flow was increased to 5.25 $L\,h^{-1}$, and the furnace was heated to 800 °C. Carbonization was started with a propene flow of 1.75 $L\,h^{-1}$ and an $N_2$ flow of 5.25 $L\,h^{-1}$ and was maintained for 7 min at 800 °C. After cooling to room temperature for 20 min under $N_2$, a shiny black alumina membrane was obtained.

**Characterization**: $^{57}$Fe Mössbauer studies were performed with a constant-acceleration-type Mössbauer spectrometer equipped with a 1024-channel analyzer operating in the timescale mode, and a 25 mCi $^{57}$Co/Rh source. The isomer shifts reported here are relative to $\alpha$-Fe at room temperature. The variable temperature spectra were recorded by means of a combined He continuous flow/bath cryostat.

TEM was performed on a Philips CM200 FEG with super twin-lens system on copper grids. Raster electron microscopy (REM) was performed on a Zeiss DSM 962 instrument. TM-AFM (tapping mode atomic force microscopy) was performed in air by using a Digital Instruments Nanoscope IIIa Multimode AFM with a maximum scan range of $10 \times 10\ \mu m^2$. Silicon cantilevers (Olympus) with resonance frequencies between 250–270 kHz, force constants of 40–50 $N\,m^{-1}$, a half cone angel of 12–14°, and tip apex radii better than 10 nm were used. The topographical images were acquired with $512 \times 512$ pixels at scan rates of 1–2 Hz. For image processing, they were flattened by the 1st-order-plan-fit algorithm of the DI software. For sample preparation, the compact fiber material was slightly dispersed in pure water using an ultrasonic bath for 1 min. This dispersion was dropped on a glass substrate (RMS roughness approximately 0.2 nm), which was cleaned first in ethanol, and dried using compressed gas (DustOff, Falcon, Inc.). By this procedure, the tubes are only fixed due to water capillary forces between the fiber surface and a thin water layer covering the glass substrate in air.

Electron energy loss spectroscopy (EELS) was performed on a Gatan PEELS 666 hooked onto a Philips CM30-ST microscope. Acceleration voltage was 300 kV ($LaB_6$-cathode). The carbon edges were measured with a resolution of 0.9 eV.

Resonance Raman studies were performed with an U1000 (ISA) spectrograph equipped with 1200 lines $mm^{-1}$ gratings and a liquid-nitrogen-cooled CCD camera. The spectral bandwidth was 3 $cm^{-1}$, the increment per data point was approximately 0.3 $cm^{-1}$, and the stability of the monochromator was found to be better than 0.1 $cm^{-1}$. The powdered sample was placed in an EPR tube and excited with the 514 nm line of an Ar laser with approximately 150 mW at ambient temperature. To improve the signal-to-noise ratio, consecutively measured spectra in the range of 800–2000 $cm^{-1}$ were finally combined to yield a total integration time of 500 s. After removal of the structureless background by polynomial subtraction, the spectrum was analyzed by a band-fitting procedure using Lorentzian lineshapes.

FESM was performed in a modified UHV-Escalab system with a three-dimensional sample scanning unit and adjustable tungsten needles.

Laser structuration was performed with a Lambda LPX210i with an average laser power of 70 W, a maximum laser repetition rate of 100 Hz, and a maximum laser pulse energy of about 700 mJ. Two separated optical configurations can be used. Laser patterning with an optical resolution of about 2 μm was obtained by a demagnification (4:1, 10:1 or 15:1) of mask structures with quartz lenses. High lateral optical resolutions of about 500 nm $\mu m^{-1}$ were obtained with Schwartzschild reflecting optics (demagnification 15:1, 25:1 or 36:1). Both optical configurations can be used with beam homogenizers. The maximum attainable laser fluence is in the range of 40 $J\,cm^{-2}$. The laser fluence is controlled by a motorized attenuator. The substrate surface could be moved below the laser beam with a positioning system in the $x$, $y$, and $z$ direction with an accuracy of $\pm 1$ μm for a travelling distance of 25 mm. The maximum travelling distances were 150 mm ($x$), 150 mm ($y$), and 5 mm ($z$), with a maximum speed of 100 mm $s^{-1}$ or 1 mm $s^{-1}$ in the $z$ direction. Furthermore, a rotating axis was fitted onto the table for precise positioning of marked surfaces.

## Acknowledgements

Financial support through the DFG (Heisenberg Fellowship to JJS), the Fonds der Chemischen Industrie, and the Dr. Heinrich Jörg Stiftung of the University of Graz is acknowledged with gratitude. Thanks are due to Dr. C. W. Lehmann (MPI für Kohlenforschung, Mülheim a.d. Ruhr) for the XRD studies and Prof. Dr. M. Fröba (University of Nürnberg-Erlangen) for BET measurements. Use of the microscopy facilities in the laboratories of Prof. G. Schmid and Prof. M. J. Setzer at the University of Essen is acknowledged with gratitude. The hydrogen storage capacity of the graphite nanostructure was measured at the ZAE Bayern, Garching, Germany, under contract No. ZAE1/99/094. We thank one of the reviewers for the coinage of the expression "nanotube bags".

[1] a) *Carbon Nanotubes, Preparation and Properties* (Ed.: T. W. Ebbesen), CRC Press, Boca Raton, **1997**; b) M. Terrones, W. K. Hsu, H. W. Kroto, D. M. R. Walton, *Top. Curr. Chem.* **1999**, *199*, 189.
[2] M. Endo, C. Kim, K. Nishimura, T. Fujino, K. Miyashita, *Carbon* **2000**, *38*, 183.
[3] G. Che, B. B. Lakshimi, E. R. Fisher, C. R. Martin, *Nature* **1998**, *393*, 346.
[4] A. C. Dillon, K. M. Jones, T. A. Bekkedahl, C. H. Kiang, D. S. Bethune, M. J. Heben, *Nature* **1997**, *386*, 377.
[5] A. Chambers, C. Park, R. T. K. Baker, N. M. Rodriguez, *J. Phys. Chem. B* **1998**, *102*, 4253.
[6] S. Lach, C. Ziegler, *Chem. Unsere Zeit*. **2000**, *34*, 58.
[7] C. Liu, Y. Y. Fan, M. Liu, H. T. Cong, H. M. Cheng, M. S. Dresselhaus, *Science* **1999**, *286*, 1127.
[8] P. Chen, X. Wu, J. Lin, K. L. Tan, *Science* **1999**, *285*, 91.
[9] a) Y. Saito, S. Uemura, K. Hamaguchi, *Jpn. J. Appl. Phys.* **1998**, *37*, 346; b) W. B. Choi, D. S. Chung, J. H. Kang, H. Y. Kim, Y. W. Jin, I. T. Han, Y. H. Lee, J. E. Jung, N. S. Lee, G. S. Park, J. M. Kim, *Appl. Phys. Lett.* **1999**, *75*, 3129.
[10] a) Y. Saito, S. Uemura, *Carbon* **2000**, *38*, 169; b) S. Fan, M. G. Chapline, N. R. Franklin, T. W. Tombler, A. M. Cassell, H. Dai, *Science* **1999**, 283, 512.
[11] M. Stammler, J. Ristein, T. Habermann, A. Göhl, K. Janischowsky, D. Nau, G. Müller, L. Ley, *Diamond Relat. Mater*. **1999**, *8*, 792.
[12] T. Kyotani, N. Sonobe, A. Tomita, *Nature* **1988**, *331*, 331.
[13] N. Sonobe, T. Kyotani, Y. Hishiyama, M. Shiraishi, A. Tomita, *J. Phys. Chem.* **1988**, *92*, 7029.
[14] W. Z. Li, S. S. Xie, L. X. Qian, B. H. Chang, B. S. Zou, W. Y. Zou, R. A. Zhao, G. Wang, *Science* **1996**, *274*, 1701.
[15] T. Kyotani, L.-F-Tsai, A. Tomita, *Chem. Mater.* **1996**, *8*, 2109.
[16] C. R. Martin, *Science* **1994**, 266, 1961.

  0947-6539/01/0713-2894 $ 17.50+.50/0 

[17] G. Che, B. B. Lakshmi, C. R. Martin, E. R. Fisher, R. S. Ruoff, *Chem. Mater*. **1998**, *10*, 260.
[18] Important work on aligned CNT synthesis: a) J. Li, C. Papadopoulos, J. M. Xu, M. Moskovits, *Appl. Phys. Lett*. **1999**, *75*, 367; b) W. Z. Li, S. S. Xie, L. X. Qian, B. H. Chang, B. S. Zou, W. Y. Zjou, R. A. Zhao, G. Wang, *Science* **1996**, *274*, 1701; c) M. Terrones, N. Grobert, J. Olivares, J. P. Zhang, H. Terrones, K. Kordatos, W. K. Hsu, J. P. Hare, P. D. Townsend, K. Prasides, A. K. Cheetham, H. W. Kroto, D. R. M. Walton, *Nature* **1997**, *388*, 52; d) C. N. R. Rao, R. Sen, B. C. Satishkumar, A. Govindaraj, *Chem. Commun*. **1998**, 1525; e) B. C. Satishkumar, A. Govindarj, R. Sen, C. N. R. Rao, *Chem. Phys. Lett*. **1998**, *293*, 47; f) S. Huang, A. Mau, W. H. Turney, P. A. White, L. Dai, *Phys. Chem*. *B* **2000**, *104*, 2193; g) Z. F. Ren, Z. P. Huang, J. W. Xu, J. H. Wang, P. Bush, M. P. Siegal, P. N. Provencio, *Science* **1998**, *282*, 1105; h) H. Kind, J. M. Bonard, C. Emmenegger, L.-O. Nilsson, K. Hernadi, E. M. Schaller, L. Schlapbach, L. Forro, K. Kern, *Adv. Mater.* **1999**, *11*, 1285; l) J. Kong, H. T. Soh, A. M. Cassell, C. F. Quate, H. Dai, *Nature* **1998**, *395*, 878; m) P. M. Ajayan, O. Stephan, C. Colliex, D. Trauth, *Science* **1994**, *265*, 1212; n) M. Terrones, N. Grobert, J. Olivares, J. P. Zhang, H. Terrones, K. Kordatos, W. K. Hsu, J. P. Hare, P. D. Townsend, K. Prasides, A. K. Cheetham, H. W. Kroto, D. R. M. Walton, *Nature* **1997**, *388*, 52; o) W. Z. Li, S. S. Xie, L. X. Qian, B. H. Chang, B. S. Zhou, W. Y. Zhou, R. A. Zhao, G. Wang, *Science* **1996**, *274*, 1701.
[19] a) J. J. Schneider, G. L. Hornyak, N. Czap, K. M. Jones, F. S. Hasoon, M. J. Heben, *Nanostruct. Mater*. **1999**, *12*, 83; b) J. J. Schneider, J. Hagen, N. Czap, J. Engstler, J. Ensling, P. Gütlich, U. Reinoehl, H. Bertagnolli, F. Luis, L. Jos de Jongh, M. Wark, G. Grubert, G. L. Hornyak, R. Zanoni, *Chem. Eur. J.* **2000**, *6*, 4305.
[20] P. Chen, H.-B. Zhang, G.-D. Lin, Q. Hong, K. R. Tsai, *Carbon* **1997**, *35*, 1495.
[21] a) W. Pfleging, A. Ludwig, K. Seemann, R. Preu, H. Mäckel, S. W. Glunz, *Appl. Surf. Sci.* **2000**, *154*, 633; b) W. Pfleging, A. Meier, T. Hanemann, H. Gruhn, K.-H. zum Gahr in *Laser-Solid Interactions for Materials Processing, Proceedings of the MRS Spring 2000* Meeting, San Francisco, USA, **2000**, in press.
[22] a) S. Amelinckx, X. B. Zhang, D. Bernaerts, X. F. Zhang, V. Ivanov, J. B. Nagy, *Science* **1994**, *265*, 635; b) H. P. Boehm, *Carbon* **1973**, *11*, 583.
[23] G. Che, B. B. Lakshmi, E. R. Fisher, C. R. Martin, *Nature* **1998**, *393*, 346.
[24] a) R. T. K. Baker, P. S. Harris, F. S. Feates, R. J. Waite, *J. Catal*. **1978**, *26*, 51; b) R. T. K. Baker, J. J. Chludzinski, Jr., *J. Catal*. **1980**, *64*, 464.
[25] a) D. Baernerts, X. B. Zhang, X. F. Zhang, S. Amelinckx, G. Van Tendeloo, J. Van Landuyt, V. Ivanov, J. B. Nagy, *Philos. Mag. A* **1995**, *71*, 605; b) V. Ivanov, J. B. Nagy, Ph. Lambin, A. Lucas, X. B. Zhang, X. F. Zhang, D. Bernaerts, G. Van Tendeloo, S. Amelinckx, V. Van Landuyt, *Chem. Phys. Lett*. **1994**, *223*, 329.
[26] a) N. G. Chopra, L. X. Benedict, V. H. Crespi, M. L. Cohen, S. G. Louie, A. Zettl, *Nature* **1995**, *377*, 135; b) T. Hertel, R. E. Walkup, P. Avouris, *Phys. Rev. B* **1998**, *58*, 13870.
[27] J. Li, C. Papadopoulos, J. Xu, *Nature* **1999**, *402*, 254.
[28] For an overview of related problems see: http://www.weizmann.ac.il/surflab/peter/
[29] Y. Wang, D. C. Alsmeyer, R. L. McGreery, *Chem. Mater*. **1990**, *2*, 557.
[30] S. S. Xie, B. H. Chang, W. Z. Li, Z. W. Pan, L. F. Sun, J. M. Mao, X. H. Qian, W. Y. Zhou, *Adv. Mater*. **1999**, *11*, 1135.
[31] a) M. Knupfer, T. Pichler, M. S. Golden, J. Fink, A. Rinzler, R. E. Smalley, *Carbon* **1999**, *37*, 733; b) V. P. Dravid, X. Lin, Y. Wang, X. K. Wang, A. Yee, J. B. Ketteson, R. P. H. Chang, *Science* **1993**, *259*, 1601; c) P. M. Ajayan, S. Iijima, T. Ichinashi, *Phys. Rev. B* **1993**, *47*, 6859.
[32] The experimental set up and further results towards gravimetric hydrogen absorption analysis of various carboneous materials are described in: *Ergebnisse des Expertenworkshops "Nanoröhren"*, VDI-Technologiezentrum Physikalische Technologien, Düsseldorf, **1998**, p. 113.

Received: July 4, 2000
Revised: January 15, 2001 [F2581]